

Assignment of Aluminum Corroles Absorption Bands to Electronic Transitions by Femtosecond Polarization Resolved VIS-Pump IR-Probe Spectroscopy

Yang Yang,[†] Dagmar Jones,[†] Theodore von Haimberger,[†] Martin Linke,[†] Linn Wagnert,[‡] Alexander Berg,[‡] Haim Levanon,[‡] Angelica Zacarias,^{†,§} Atif Mahammed,^{||} Zeev Gross,^{||} and Karsten Heyne^{*,†}

[†]Department of Physics, Freie Universität Berlin, Arnimallee 14, 14195 Berlin, Germany

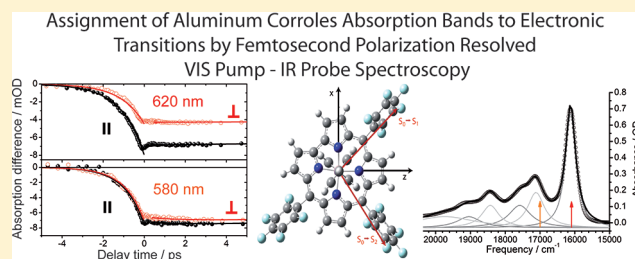
[‡]Institute of Chemistry, The Hebrew University of Jerusalem, Jerusalem 91904, Israel

[§]Max-Planck-Institut für Mikrostrukturphysik and European Theoretical Spectroscopy Facility (ETSF), Weinberg 2, 06120 Halle, Germany

^{||}Schulich Faculty of Chemistry, Technion-Israel Institute of Technology, Haifa 32000, Israel

 Supporting Information

ABSTRACT: We combine femtosecond polarization resolved VIS-pump IR-probe spectroscopy with DFT and TD-DFT calculations to identify and assign absorption bands to electronic transitions for corroles. These macrocycles and their corresponding metal complexes are receiving great attention because of their utility in many fields, while many of their spectroscopic features have not yet been fully described. Analysis of the perturbed free induction decay provides information about the bleaching signal at time zero and allows for determination of overlapping excited state and bleaching signal amplitudes. The $S_0 \rightarrow S_1$ and $S_0 \rightarrow S_2$ transitions in the Q-band of the hexacoordinated $\text{Al}(\text{tpfc})(\text{py})_2$ and $\text{Br}_8\text{Al}(\text{tpfc})(\text{py})_2$ absorption spectra are explicitly assigned. Angles between these electronic transition dipole moments (tdms) with a single vibrational transition dipole moment of $(53 \pm 2)^\circ$ and $(34 \pm 2)^\circ$ when excited at 580 and 620 nm for hexacoordinated $\text{Al}(\text{tpfc})(\text{py})_2$ and $(51 \pm 2)^\circ$ and $(43 \pm 2)^\circ$ when excited at 590 and 640 nm for hexacoordinated $\text{Br}_8\text{Al}(\text{tpfc})(\text{py})_2$ were determined. The relative angles between the two lowest electronic tdms are $(90 \pm 8)^\circ$ and $(94 \pm 3)^\circ$ for $\text{Al}(\text{tpfc})(\text{py})_2$ and $\text{Br}_8\text{Al}(\text{tpfc})(\text{py})_2$, respectively. Angles are determined before time zero by polarization resolved perturbed free induction decay and after time zero by polarization resolved transients. Comparison of corrole's wave functions with those of porphine show that the reduced symmetry in the corrole molecules results in lifting of Q-band degeneracy and major reorientation of the electronic transition dipole moments within the molecular scaffold. This information is necessary in designing optimal corrole-based electron and energy transfer complexes.



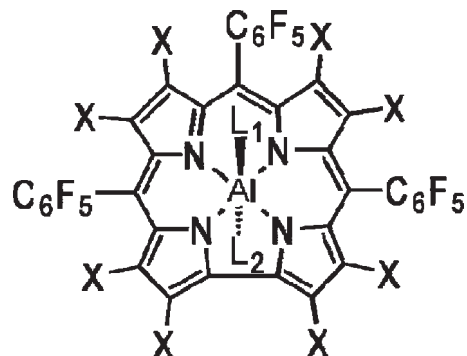
INTRODUCTION

The UV/vis absorption profile of a photoactive molecule is a key property, indicating electronic structure and interaction with its surrounding. Time-resolved spectroscopy in this spectral range allows for the elucidation of time constants of reactions and relaxation processes, as well the determination of individual transient absorption profiles. In most cases, absorption profiles exhibit different transition dipole orientations, and their relative orientations can be measured by polarization resolved spectroscopy. Unfortunately, excited state absorption spectra (ESA) often have very broad and complex profiles that impede differentiation of $S_1 \rightarrow S_2$ ESA from other transitions. For molecules with various excited state transitions, e.g., porphyrins, a complex transient pattern of absorption spectra occurs that is barely identifiable. One reason for the complexity of transient excited state spectra is the well-known degeneracy of the Q transition dipole moments μ_{el} of porphyrins.^{1,2} Lifting of the degeneracy

can be induced by symmetry breaking, e.g., as in Chl *a*, but it is not known whether corroles that possess one meso-group less than porphyrins shows degeneracy of the Q-band. The Q-band absorption of corroles ranges from 450 to 650 nm, similar to the porphyrins. Subband heads and their vibronic progressions are visible in the whole spectral range. Corroles are an emerging class of photoactive molecules with remarkable chemical and photochemical properties and relatively unexplored potential.^{3–7} The development of a simple and efficient procedure of corroles synthesis^{8,9} combined with readily tuned physical and chemical characteristics over a wide range by varying the peripheral substituents, axial ligands, and central metal has revived substantial interest in employing these porphyrinoids in various fields.¹⁰ Examples for utilization of the corroles include

Received: December 12, 2011

Published: December 27, 2011

Scheme 1. Structure of the Corrole Molecules Investigated^a

^a L₁ and L₂ denote axial ligands. Al(tpfc)(py)₁: L₁ = pyridine, no L₂, X = H. Al(tpfc)(py)₂: L₁ = L₂ = pyridine, X = H. Br₈Al(tpfc)(py)₁: L₁ = pyridine, no L₂, X = Br. Br₈Al(tpfc)(py)₂: L₁ = L₂ = pyridine, X = Br.

dye-sensitized solar cells,¹¹ photodynamic detection,¹² regular and sophisticated optical imaging,¹³ formation of singlet oxygen for catalysis,¹⁴ photodynamic therapy,^{15–17} and corrole-based electron and energy transfer systems.¹⁸ In this context, the ability to control the corrole's parameters such as quantum yield, energy, and lifetime of their photoexcited state is fundamental in optimizing corrole-based photocatalysts for their specific application.^{7–12} The intense fluorescence of gallium(III) corroles has also been used for animal, organ, and cellular imaging as an important tool for evaluating the bioavailability of the nonfluorescent iron(III) and manganese(III) complexes that are successfully used in a variety of disease models that are caused by oxidative stress.^{19,20} However, there are very few in-depth reports on the physical and spectroscopic features of corroles.²¹ The most striking example is vibrational spectroscopy (IR, RR, and more sophisticated methods), which is well established for porphyrins and of practically zero knowledge for corroles. An improved insight into the fundamental properties of post-transition metallocorroles is hence clearly necessary to fully realize their potential practical applications.

Here, we focus on the peculiarities of electronic transitions in the Q-band since properties of corrole-based electron donor–acceptor complexes are governed by the frequency dependent interaction of their electronic transitions. Femtosecond polarization resolved UV-vis-pump IR-probe spectroscopy is used to determine the angle between the excited electronic transition dipole moment μ_{el} and a single vibrational transition dipole moment μ_{vib} within the corrole molecule investigated. Excitation at different frequencies within the absorption spectrum reveals different angles (μ_{el} and μ_{vib}) indicating different excited electronic transition dipole moments. We investigated the lowest electronic transitions of the Q-band of hexacoordinated aluminum(III) S_{10,15}-tris(pentafluorophenyl) corrole molecules, Al(tpfc)(py)₂^{22–25} and Br₈Al(tpfc)(py)₂²⁵ drawn in Scheme 1. Al(tpfc)(py)₂ exhibits high fluorescence quantum yield and shows no triplet dynamics in time-resolved EPR experiments, in contrast to Br₈Al(tpfc)(py)₂.²⁵ Consequently, in strongly interacting corrole-based donor–acceptor complexes, we would expect a remarkable contrast due to major depletion of the high fluorescence.

■ EXPERIMENTAL SECTION

Sample Preparation. The Al(tpfc)(py)₂ and Br₈Al(tpfc)(py)₂ were synthesized as reported previously.^{22,25} Corrole samples of

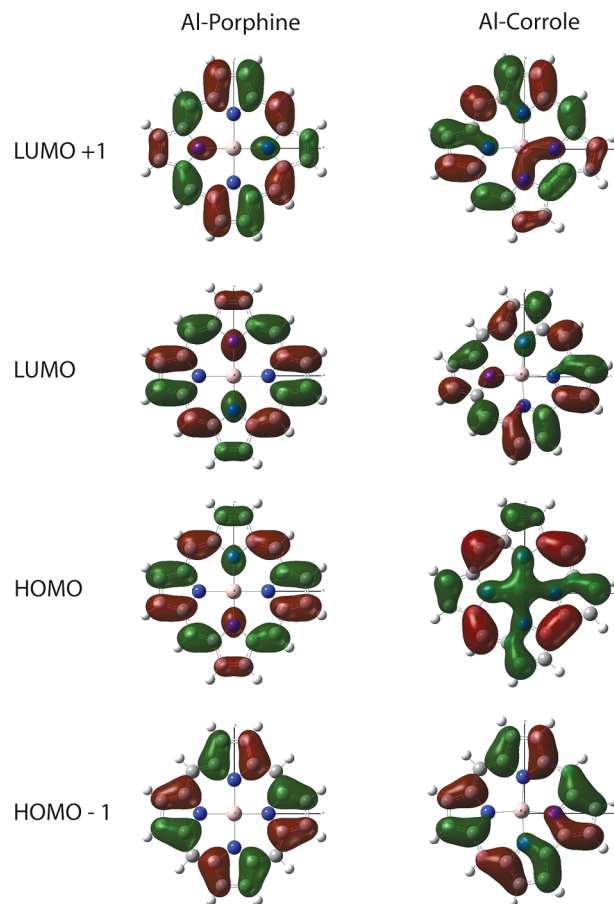


Figure 1. Left: Al-porphine wave functions. Right: Al-corrole wave functions.

0.004 mol/L of Al(tpfc)(py)₂ and Br₈Al(tpfc)(py)₂ in *d*₈-toluene were prepared with a maximal absorption of about 0.6 OD in the Q-band (Figures 1 and 2). As vibrational reference transition dipole moment orientation, we chose the vibrational transition at 1519 cm⁻¹ in Al(tpfc)(py)₂ and 1521 cm⁻¹ in Br₈Al(tpfc)(py)₂ tentatively assigned to a C=C stretch vibration in the molecular plane, respectively. The infrared absorption of this vibration was about 150 mOD as presented in Figure 3.

Quantum Calculations. All the quantum-chemical calculations were done with Gaussian09.²⁶ Geometry optimization of the corroles, vibrational frequency calculations, and determination of the μ_{vib} orientations in the molecular scaffold were performed with density functional theory (DFT)²⁷ using the B3LYP exchange-correlation functional and the 6-31G** basis set. The electronic transition energies, corresponding oscillator strengths, and transition dipole orientations were calculated with time-dependent density functional theory (TD-DFT)²⁸ at the same level of theory.

HOMO and LUMO Wave Functions Analysis. While the frontier orbitals of corroles have been reported in many publications,^{29–31} little attention was devoted to the relevant electronic transitions. To throw light upon the nature of these transitions and their relation to the electron degeneracy, we analyze in detail the orbital contributions for the bare Al-corrole ring and Al-porphine ring, the last was calculated as a doublet and a net charge of zero.

Our analysis of the molecular orbitals (MO) associated to the respective excitations shows that the transition S₀ → S₁ is

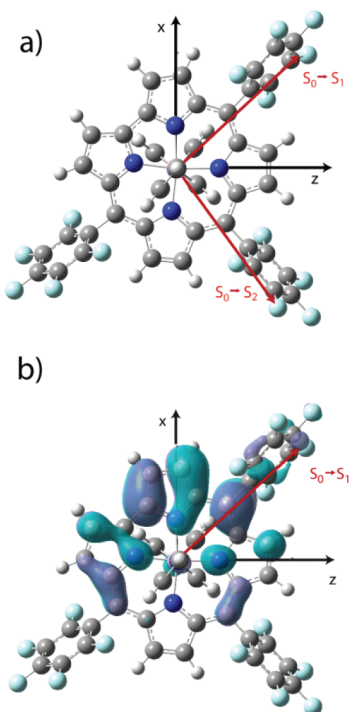


Figure 2. Structural model of Al(tpfc)(py)₂ from DFT calculations. (a) The red arrows show the TD-DFT calculated directions for the electronic transition moments. (b) Difference of the HOMO and LUMO orbitals contributing to the S₀ → S₁ μ_{el} (red arrow); colored surfaces indicate regions with equal electron densities.

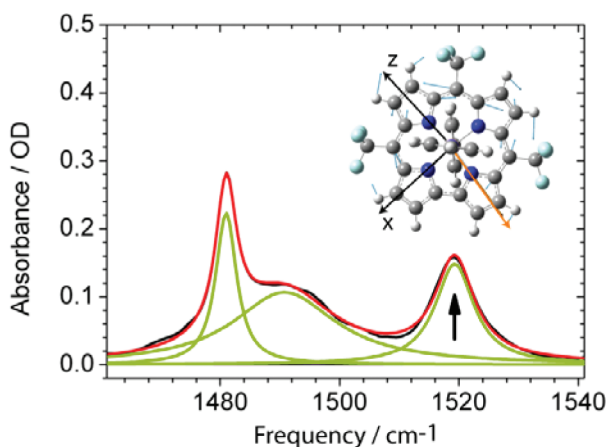


Figure 3. Vibrational absorption spectrum of Al(tpfc)(py)₂ in toluene (black line). The simulated absorption spectrum (red line) is given by a sum of three Lorentzian lines (green lines), pyridine absorption at 1480 cm⁻¹, and two C=C stretching vibrations at 1491 cm⁻¹ and 1519 cm⁻¹. The spectral line width of the vibration at 1519 cm⁻¹ is 7.9 cm⁻¹. Inset: Structural model of Al(III)-(trifluoromethyl)corrole with two pyridine ligands. Atomic displacements due to a C=C stretching vibration are given by blue arrows, the vibrational transition dipole moment by an orange arrow. Note that transition dipole moment vectors point in either directions.

associated to a HOMO → LUMO electron transfer, while the transition S₀ → S₂ corresponds to a combination of an electron transfer between HOMO - 1 → LUMO and HOMO → LUMO + 1. The nature of these orbitals shows that these excitations are not

equivalent, as we can see from Figure 1 where it is clearly seen that the role of the Al varies from HOMO to HOMO - 1 drastically, and therefore, an electronic transition between HOMO and LUMO would be of different nature as a transition between HOMO - 1 and LUMO.

Figure 1 displays the MO for these systems. The orbital distribution for the Al-porphine (Figure 1 left) is strictly symmetric, and the calculation of the μ_{el} for the two lowest electronic singlet excitations shows that they orient along each one of the N-Al-N axes. The orientation of the μ_{el} for the Al-corrole and the MO distributions (see Figure 1 right) show that the symmetry axis of these excitations is no longer along the N-Al-N axis. The missing meso-bridge in this molecule produces a change in the symmetry behavior drastically resulting in a rotation of the μ_{el} s such that the μ_{el} s orientations are mainly parallel or perpendicular to the axis along the Al and the missing meso-bridge. The impact of the missing meso-bridge in corroles lead to more property changes compared to Chl *a*, where the Q-band electronic transition dipole moments show lifted degeneracy, but their orientations are predominantly along the N-Mg-N axis.³²

Although going from the totally symmetric Al-porphine ring to the Al-corrole ring and its substituted analogue corrole systems reduces the symmetry of the orbital electron density, the analysis of their MOs and μ_{el} s correlates in the same fashion as for the nonsubstituted Al-corrole ring molecule.

Femtosecond VIS-Pump IR-Probe Experiments. Polarization resolved femtosecond (fs) VIS-pump IR-probe experiments were performed on Al(tpfc)(py)₂ and Br₈Al(tpfc)(py)₂ with linear polarized fs excitation pulses at 580 and 620 nm and 590 and 640 nm, respectively, far away from saturation. The pump pulse excites about 6% of the molecules in isotropic solution and photoselects predominantly the corrole molecules with their μ_{el} oriented parallel to the polarization of the pump beam. Since the μ_{el} and the μ_{vib} are characterized by fixed orientations within the molecular scaffold, μ_{el} s with different orientations exhibit different angles Θ to the μ_{vib} . We probed the μ_{vib} with fs mid-infrared pulses polarized parallel and perpendicular to the pump pulse polarization, in the range from 1500 cm⁻¹ to 1540 cm⁻¹ with a spectral resolution of 1.5 cm⁻¹. Pump pulses were generated by a collinear multistage optical parametric amplifier (OPA) setup³³ and probe pulses by a collinear OPA setup followed by difference frequency generation.³⁴ The time resolution (system response) of the experiment was below 350 fs.

RESULTS AND DISCUSSION

Theoretical TD-DFT calculations predict two μ_{el} s in the Q-band region. The S₀ → S₁ transition is calculated at 17 800 cm⁻¹, with $\mu_1 = (0.9990/-0.0306/1.0876)$, while μ_{el} coordinates of the S₀ → S₂ transition at 18 600 cm⁻¹, with μ_{el} coordinates of $\mu_2 = (0.1688/0.0268/-0.1200)$. Both μ_{el} s lie predominantly in the molecular plane of the corrole moiety as shown in Figure 2. Taking into account a constant energy offset of 1630 cm⁻¹ for the calculations, the computed frequency positions agree well with the experimental values. For Br₈Al(tpfc)(py)₂, we calculated μ_{el} coordinates of $\mu_{\text{Br},1} = (-1.0577/0.0091/-0.9040)$ for the S₀ → S₁ transition at 17 450 cm⁻¹ and of $\mu_{\text{Br},2} = (0.4056/0.1181/-0.4703)$ for the S₀ → S₂ transition at 18 250 cm⁻¹. Upon bromination, a calculated reduction of the HOMO-LUMO energy gap of 350 cm⁻¹ is observed.

The angle between μ_1 and μ_2 is calculated to be 83° for Al(tpfc)(py)₂ and 90° for the Br₈Al(tpfc)(py)₂. They differ by 7°.

Polarization Resolved fs VIS-Pump IR-Probe Spectroscopy. Femtosecond time-resolved polarization resolved VIS-pump IR-probe spectroscopy allows to calculate the relative angle Θ between a μ_{vib} and μ_{el} .^{32,35,36} As the reference vibration, we chose the prominent vibrational absorption at 1519 cm^{-1} in Al(tpfc)-(py)₂ and 1521 cm^{-1} in Br₈Al(tpfc)(py)₂ assigned as a structure-sensitive marker band.³⁷ By calculations, we assign this vibration to a C=C stretch vibration lying predominantly in the molecular plane. Steady-state FTIR absorption spectra reveal Lorentzian line widths of the C=C stretching vibration of $(7.9 \pm 0.5) \text{ cm}^{-1}$ and $(5.4 \pm 0.5) \text{ cm}^{-1}$ for Al(tpfc)(py)₂ and Br₈Al(tpfc)(py)₂, respectively. Ground state DFT calculations on a model correlate locate the μ_{vib} orientation predominantly along the z axis (Figure 3).

The angle Θ between a μ_{vib} and a μ_{el} is evaluated by the dichroic ratio D ($D = A_{||}/A_{\perp}$, with $A_{||}$ and A_{\perp} being the absorption change for parallel and perpendicular polarization, respectively, and $\Theta = \arccos[(2D - 1)/(D + 2)]^{1/2}$). Pump pulses with widths of about 10 nm were located at 580 and 620 nm for Al(tpfc)(py)₂ and at 590 and 640 nm for Br₈Al(tpfc)(py)₂.

Perturbed Free Induction Decay. Transient measurements were used to analyze the dynamics and the perturbed free induction decay (PFID).³⁸ The PFID is a coherent effect, where the IR probe pulse induces a polarization on the vibrational mode that is perturbed by the delayed pump pulse. No net absorption of the probe pulse occurs in this case, but a frequency dependent modulation pattern is imprinted on the probe pulse intensity.^{39–41} At the center of a single Lorentzian bleaching band, the PFID signal is given by the Fourier transformation of the spectral line shape, i.e., a single exponential decay. Determination of the exponential decay time constant requires a spectral resolution much higher than the absorption band line width. The modulation pattern occurs before the pump pulse arrives and has no relationship with the photo-induced dynamics of the molecule. Since the molecule is in its ground state, the PFID can be used to determine ground state properties like the amplitude of the bleaching absorption and the angle θ between μ_{el} and μ_{vib} . This makes possible an accurate calculation of the amplitude of overlapping excitation and bleaching bands as found in the dynamics studied in this article.

The C=C stretch vibrational absorption band of Al(tpfc)-(py)₂ exhibits a perturbed free induction decay at 1519 cm^{-1} with a dephasing time constant τ_2 of 1.1 ps and a 1σ error margin of 0.2 ps determined by Exhaustive Search Analysis (ExSeAn) at excitation at 620 nm (Figure 6 upper panel).⁴² The PFID amplitude signals and error ranges are given in Table S1, Supporting Information. As expected, the excitation at 580 nm produced similar values for the dephasing time τ_2 of 1.0 ps and a 1σ error margin of 0.2 ps by ExSeAn. The dephasing time corresponds to a natural line width of $(9 \pm 2) \text{ cm}^{-1}$, in agreement with the line width observed in the vibrational absorption spectrum (Figure 3).^{39,40} Thus, we conclude that at 1519 cm^{-1} , only this vibrational absorption is responsible for the measured signal and provides a suitable vibrational reference transition dipole moment (μ_{vib}) to determine its relative angle to μ_{el} .

With the dichroic ratio of the amplitudes of the PFID signals presented in Figure 4, the relative angle θ between μ_{vib} and $S_0 \rightarrow S_1$ electronic transition dipole moment $\mu_{\text{el}01}$, as well as $S_0 \rightarrow S_2$ electronic transition dipole moment $\mu_{\text{el}02}$, is determined. In Al(tpfc)(py)₂, we found angles of $(34 \pm 2)^\circ$ and $(53 \pm 2)^\circ$ for $(\mu_{\text{vib}}, \mu_{\text{el}01})$ and $(\mu_{\text{vib}}, \mu_{\text{el}02})$, respectively. For both polarizations, the amplitudes of the PFID signal calculated at time zero represent the peak height of the bleaching signal of the C=C stretch vibration. Since we are only able to measure

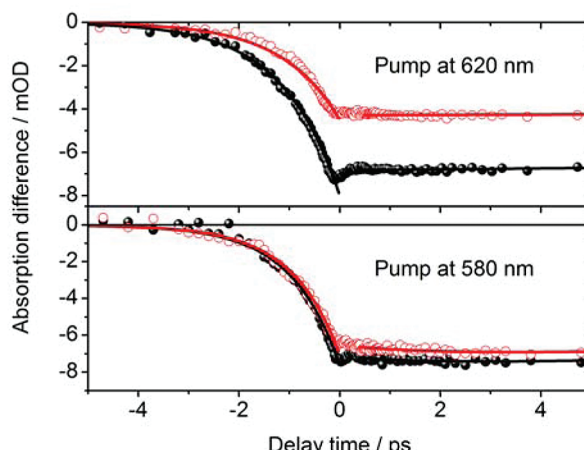


Figure 4. Polarization resolved transients of Al(tpfc)(py)₂ at 1519 cm^{-1} after excitation at 620 nm (upper panel) and 580 nm (lower panel). Parallel polarization (black circles) and perpendicular polarization (red circles) with respect to pump pulse polarization. Red and black lines before delay time zero indicate PFID simulations and, after time zero, transient dynamic simulations.

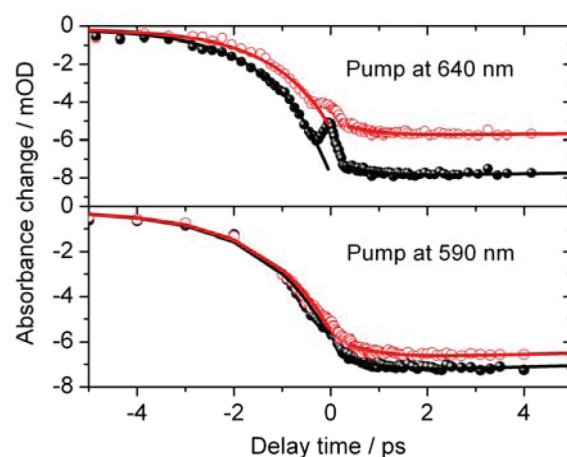


Figure 5. Polarization resolved transients of Br₈Al(tpfc)(py)₂ at 1521 cm^{-1} after excitation at 640 nm (upper panel) and 590 nm (lower panel). Parallel polarization (black circles) and perpendicular polarization (red circles) with respect to pump pulse polarization. Red and black lines before delay time zero indicate PFID simulations and, after time zero, transient dynamic simulations. The dip around time zero indicates the system response.

relative angles, we cannot decide whether the two angles are on the opposite or same side of the vibrational transition dipole moment.

For Br₈Al(tpfc)(py)₂, the C=C stretch vibrational absorption band is located at 1521 cm^{-1} with a dephasing time constant τ_2 of $(1.3 \pm 0.3) \text{ ps}$ on excitation at 640 nm (Figure 5 upper panel) and a dephasing time τ_2 of $(1.5 \pm 0.3) \text{ ps}$ on excitation at 590 nm. At time zero, the dip in the transients results from nonlinear effects indicating the system response. The time interval of non-negligible system response contributions was not used to calculate the PFID signals. The dephasing time corresponds to a natural line width of $(7 \pm 3) \text{ cm}^{-1}$, slightly larger than the line width observed in the vibrational absorption spectrum of $(5.4 \pm 0.5) \text{ cm}^{-1}$. The deviations are due to a spectral resolution

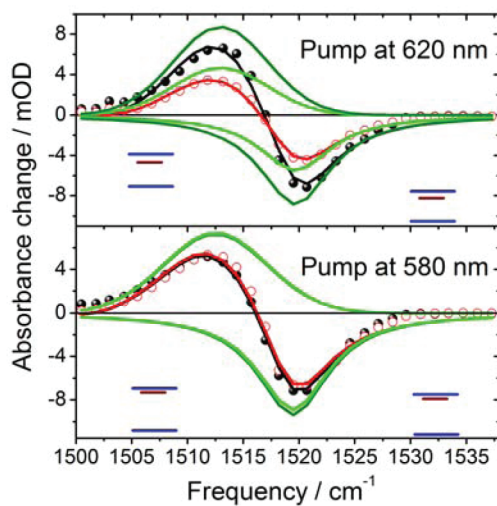


Figure 6. Polarization resolved absorbance difference spectrum (DAS) of $\text{Al}(\text{tpfc})(\text{py})_2$ calculated for time zero. Parallel polarized data (black dots); perpendicular polarized data (red circles); simulations of the positive excited state vibrational signal (Gaussian) and negative ground state bleaching signal (Lorentzian) are shown in dark green lines for parallel polarization and green lines for perpendicular polarization. Blue lines indicate 2σ error margins of the simulated bleaching amplitude for parallel and perpendicular polarization on the right and left side, respectively. Brown lines indicate the optimal amplitude of the PFID signal for parallel and perpendicular polarization. Upper panel: DAS after excitation at 620 nm. Lower panel: DAS after excitation at 580 nm.

of 1.5 cm^{-1} not high enough to measure the transient at the center of the 5.4 cm^{-1} broad C=C stretch absorption band. Spectral positions with slightly lower or higher frequency show steeper PFID slopes, shorter dephasing times, and, therefore, broader natural line widths. Thus, PFID amplitudes (Table S1, Supporting Information) match the Lorentzian fit amplitudes only within the 2σ range. We found no evidence for other contributing vibrational bands at 1521 cm^{-1} so that this vibrational absorption provides a suitable μ_{vib} reference to determine its relative angle to μ_{els} . By evaluation of the PFID signals, we determine relative angles of $(40 \pm 5)^\circ$ and $(52 \pm 3)^\circ$ for the angles $(\mu_{\text{vib}}, \mu_{\text{el}01})$ and $(\mu_{\text{vib}}, \mu_{\text{el}02})$, respectively.

Absorption Difference Spectra. The dynamics for positive delay times provide information on the signal strengths of bleaching and excited state signals. As depicted in Figures 4 and 5, the signal variations in the transients are small on a time scale of 5 ps. Simulating these dynamics by a sum of exponentials, the decay associated spectrum (DAS) at time zero is given by the amplitudes of the exponentials. Using the DAS for parallel and perpendicular polarization, the angles θ can be determined for bleaching signals and excited state signals. In Figures 6 and 7, the polarization resolved DAS for $\text{Al}(\text{tpfc})(\text{py})_2$ and $\text{Br}_8\text{Al}(\text{tpfc})(\text{py})_2$ are presented for different excitation wavelengths. The overlapping excited state absorption around 1513 cm^{-1} with the bleaching signals around 1520 cm^{-1} prevent a precise determination of the bleaching and excited state amplitudes because the measured absorption difference spectra can be simulated by the sum of positive and negative amplitudes varying in a wide range. Given the PFID amplitude and decay time, the range of the signal strength and the Lorentzian line width of the bleaching signal is limited.

Thus, excited state signal and line shape can be calculated despite the overlapping signals. For $\text{Al}(\text{tpfc})(\text{py})_2$, we found no

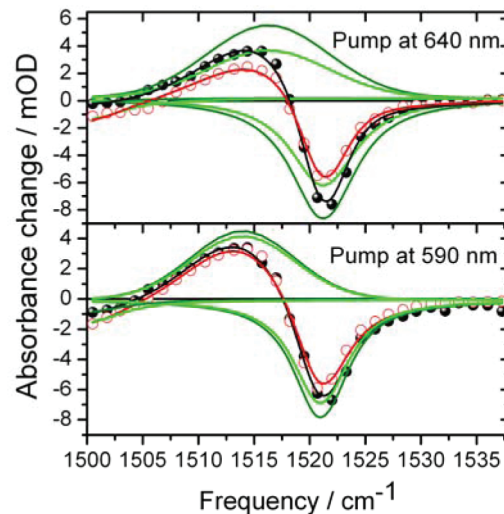


Figure 7. Polarization resolved absorbance difference spectrum (DAS) of $\text{Br}_8\text{Al}(\text{tpfc})(\text{py})_2$ calculated for time zero. Parallel polarized data (black dots); perpendicular polarized data (red circles); simulations of the positive excited state vibrational signal and negative ground state bleaching signal are shown in dark green lines for parallel polarization and green lines for perpendicular polarization. Gaussian line shapes are used for vibrations in the electronic excited state and Lorentzian line shapes in the ground state. Upper panel: DAS after excitation at 640 nm. Lower panel: DAS after excitation at 590 nm.

solution for a Lorentzian line shape matching the experimental data. A Gaussian line shape of the vibration at 1513 cm^{-1} in the excited state with a width of $(10 \pm 1) \text{ cm}^{-1}$ is in good agreement with the experimental data. Structural heterogeneities in the electronic excited state and broadening due to anharmonic couplings to other vibrations can induce the Gaussian line shape. We determined angles θ in the electronic ground state of $(37 \pm 5)^\circ$ and $(53 \pm 3)^\circ$ and in the electronic excited state of $(32 \pm 5)^\circ$ and $(54 \pm 3)^\circ$ for excitation at 620 and 580 nm, respectively.

The peak height of the C=C stretch bleaching band is given by the PFID amplitude (Table S1, Supporting Information) and is shown in Figure 6 as a brown line, for each polarization. The simulated Lorentzian bleaching band amplitude has to match this value within the 1σ or 2σ error margin. The 2σ error margins are given in Figure 6 for both polarizations (blue lines).

In $\text{Br}_8\text{Al}(\text{tpfc})(\text{py})_2$, we found angles θ in the electronic ground state of $(44 \pm 3)^\circ$ and $(50 \pm 3)^\circ$ and in the electronic excited state of $(41 \pm 5)^\circ$ and $(52 \pm 3)^\circ$ for excitation at 640 and 590 nm, respectively. The vibrational absorption in the excited state is found at $(1515 \pm 1) \text{ cm}^{-1}$ with a Gaussian width of $(11 \pm 1) \text{ cm}^{-1}$.

The presented method allows for precise measurement of the relative angle between μ_{vib} and μ_{el} . Assuming that the selected μ_{vib} and the two investigated μ_{el} orientations lie in the molecular plane, we restricted the orientations of the two electronic transition dipole moments to lie either on the same side or on opposite sides of the μ_{vib} orientation.

Simulation of the Absorption Spectrum. The Q-band absorption of $\text{Al}(\text{tpfc})(\text{py})_2$ ranges from 650 to 450 nm, or $15\ 000 \text{ cm}^{-1}$ to $20\ 000 \text{ cm}^{-1}$ as presented in Figure 8. Under low pyridine concentration, $\text{Al}(\text{tpfc})(\text{py})_2$ is in equilibrium with $\text{Al}(\text{tpfc})(\text{py})_1$. The loss of one ligand results in significant changes in the absorption spectrum as shown in Figure 8.

The isosbestic point at $16\ 520 \text{ cm}^{-1}$ indicates the existence of only two species. Transformation from $\text{Al}(\text{tpfc})(\text{py})_2$ to $\text{Al}(\text{tpfc})(\text{py})_1$

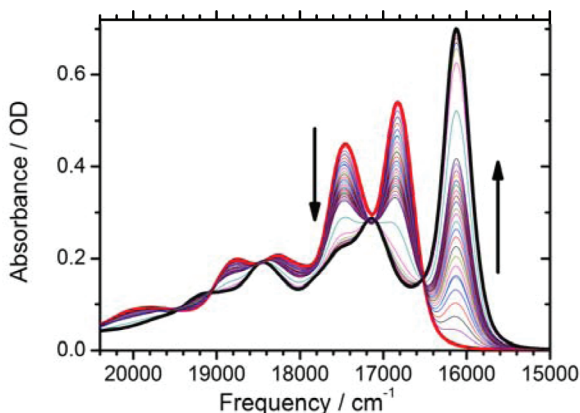


Figure 8. Absorption spectrum of the Q-band of $\text{Al}(\text{tpfc})(\text{py})_x$ in toluene upon pyridine titration ($x = 1,2$). $\text{Al}(\text{tpfc})(\text{py})_1$ absorption spectrum (red thick line); arrows indicate a signal decrease around $17\,000\text{ cm}^{-1}$ and a signal increase around $16\,000\text{ cm}^{-1}$ upon increasing pyridine concentration. $\text{Al}(\text{tpfc})(\text{py})_2$ absorption spectrum (black thick line).

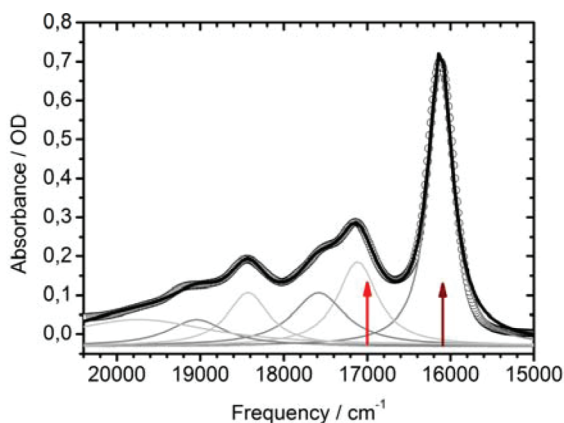


Figure 9. Absorption spectrum of $\text{Al}(\text{tpfc})(\text{py})_2$. The absorption spectrum (circles) is well simulated by a sum of six Gaussian profiles (thick black line). Red and brown arrows indicate the excitation frequencies for time-resolved experiments.

is a reversible process and results in two distinct absorption spectra for $\text{Al}(\text{tpfc})(\text{py})_2$ to $\text{Al}(\text{tpfc})(\text{py})_1$, presented in Figures 9 and Figure 8 (red thick line), respectively.^{23,24} Similar observations were made for the conversion of $\text{Br}_8\text{Al}(\text{tpfc})(\text{py})_2$ to $\text{Br}_8\text{Al}(\text{tpfc})(\text{py})_1$ (not shown). The individual absorption spectra of $\text{Al}(\text{tpfc})(\text{py})_2$ is simulated by a sum of Gaussian absorption profiles to identify possible vibronic structures.

In Figure 9, the absorption spectrum and simulated Gaussian profiles for $\text{Al}(\text{tpfc})(\text{py})_2$ are presented. Individual absorption peaks are located at $16\,120\text{ cm}^{-1}$ (P_{21}), $17\,116\text{ cm}^{-1}$ (P_{22}), $17\,582\text{ cm}^{-1}$ (P_{23}), $18\,428\text{ cm}^{-1}$ (P_{24}), $19\,044\text{ cm}^{-1}$ (P_{25}), and $19\,740\text{ cm}^{-1}$ (P_{26}) with decreasing amplitude and frequency position certainty. A single electronic 0–0 transition at $16\,120\text{ cm}^{-1}$ with vibronic substructures cannot explain the spectral profile.

The substructures in the $\text{Al}(\text{tpfc})(\text{py})_2$ Q-band absorption spectrum exhibit similar frequency differences between P_{23} and P_{21} and between P_{24} and P_{22} by 1372 cm^{-1} and 1312 cm^{-1} , respectively. This vibronic pattern of two electronic transitions can explain the complete substructure of the absorption spectrum.

CONCLUSIONS

The conclusive evidence for the existence of different electronic transitions in the Q-band spectral range of different Al-corroles was obtained using polarization resolved femtosecond VIS-pump IR-probe spectroscopy, measuring the angle between a single vibrational transition dipole moment and an electronic transition dipole moment, which are both fixed within the molecular scaffold. Detection of the polarization resolved vibrational perturbed free induction decay (PFID) allowed the determination of the angle between the electronic and vibrational transition dipole moment without influence of overlapping contributions of the electronic excited state signals. We varied the excitation frequency over the Q-band absorption spectrum and identified different angles for two different electronic transitions in the Q-band of $\text{Al}(\text{tpfc})(\text{py})_2$ and $\text{Br}_8\text{Al}(\text{tpfc})(\text{py})_2$, located at $16\,210\text{ cm}^{-1}$ ($S_0 \rightarrow S_1$) and $17\,116\text{ cm}^{-1}$ ($S_0 \rightarrow S_2$) and at $16\,640\text{ cm}^{-1}$ ($S_0 \rightarrow S_1$) and $15\,670\text{ cm}^{-1}$ ($S_0 \rightarrow S_2$), respectively. The $S_0 \rightarrow S_1$ and $S_0 \rightarrow S_2$ transitions are separated by about 950 cm^{-1} in both molecules, while the HOMO–LUMO energy gap is reduced by about 540 cm^{-1} upon bromination. Analysis of the PFID signals and decay associated spectra show relative angles between the electronic ($S_0 \rightarrow S_1$) transition dipole moment and vibrational C=C stretching transition dipole moment of $(34 \pm 2)^\circ$ and $(43 \pm 2)^\circ$ for $\text{Al}(\text{tpfc})(\text{py})_2$ and $\text{Br}_8\text{Al}(\text{tpfc})(\text{py})_2$, respectively. Upon ($S_0 \rightarrow S_2$) excitation of $\text{Al}(\text{tpfc})(\text{py})_2$ and $\text{Br}_8\text{Al}(\text{tpfc})(\text{py})_2$, we found relative angles of $(53 \pm 2)^\circ$ and $(51 \pm 2)^\circ$, respectively. The resulting angles between the two electronic transitions of $(87 \pm 4)^\circ$ and $(94 \pm 4)^\circ$ agree well with our calculated values of 83° and 90° for $\text{Al}(\text{tpfc})(\text{py})_2$ and $\text{Br}_8\text{Al}(\text{tpfc})(\text{py})_2$, respectively.

We demonstrate that the missing meso-bridge in the corrole macrocycle introduces a significant symmetry alteration in the HOMO and LUMO wave functions as compared with those of porphine resulting in lifted degeneracy and altered orientation of the electronic transition dipole moments by about 45° . These features allow for further fine-tuning of the physical and chemical features of corroles, an aspect that is crucial for their steadily growing applications in chemistry, physics, and biology.⁴³

Furthermore, the spectral location of different electronic transitions in the Q-band provides essential information for electronic interactions in corrole-based donor–acceptor and donor–spacer–acceptor systems. The results of this study will be used to identify appropriate acceptor molecules for corrole-based electron and energy transfer systems with high efficiency. Studies on those systems are underway.

ASSOCIATED CONTENT

S Supporting Information. Full listing of ref 26; C=C bleaching band amplitudes of the PFID signals and DAS spectra for both polarizations; coordinates of Al-corrole, Al-porphine, $\text{Al}(\text{tpfc})(\text{py})_2$, and $\text{Br}_8\text{Al}(\text{tpfc})(\text{py})_2$. This material is available free of charge via the Internet at <http://pubs.acs.org>.

AUTHOR INFORMATION

Corresponding Author

*E-mail: Karsten.heyne@fu-berlin.de.

ACKNOWLEDGMENT

We thank the Deutsche Forschungsgemeinschaft (HE-5206/2-1), and the e-I3 ETSF project (INFRA-2007-1.2.2: Grant Agreement

Number 211956) for financial support and the Computing Center at the FUB (ZEDAT) and MPI-Halle for further support.

■ ABBREVIATIONS

PFID, perturbed free induction decay; fs, femtosecond; tdm, transition dipole moment; MO, molecular orbital; tpfc, S_{10,15}-tris-(pentafluorophenyl) corrole; py, pyridine; TD-DFT, time-dependent density functional theory; DFT, density functional theory; ExSeAn, Exhaustive Search Analysis; OPA, optical parametric amplifier; HOMO, highest occupied molecular orbital; LUMO, lowest unoccupied molecular orbital

■ REFERENCES

- (1) Gouterman, M. *J. Chem. Phys.* **1959**, *30*, 1139–1161.
- (2) Gouterman, M. *J. Mol. Spectrosc.* **1961**, *6*, 138–163.
- (3) Rabinovich, E.; Goldberg, I.; Gross, Z. *Chem.—Eur. J.* **2011**, *17*, 12294–12301.
- (4) Vestfried, J.; Botoshansky, M.; Plamer, J. H.; Durrell, A. C.; Gray, H. B.; Gross, Z. *J. Am. Chem. Soc.* **2011**, *133*, 12899–12901.
- (5) Aviv, I.; Gross, Z. *Chem. Commun.* **2007**, 1987–1999.
- (6) Czarnecki, K.; Nimri, S.; Gross, Z.; Proniewicz, L. M.; Kincaid, J. R. *J. Am. Chem. Soc.* **1996**, *118*, 2929–2935.
- (7) Paolesse, R. *Synlett* **2008**, *15*, 2215–2230.
- (8) Gross, Z.; Galili, N.; Simkhovich, L.; Saltsman, I.; Botoshansky, M.; Blaser, D.; Boese, R.; Goldberg, I. *Org. Lett.* **1999**, *1*, 599–602.
- (9) Paolesse, R.; Jaquinod, L.; Nurco, D. J.; Mini, S.; Sagone, F.; Boschi, T.; Smith, K. M. *Chem. Commun.* **1999**, *14*, 1307–1308.
- (10) Aviv-Harel, I.; Gross, Z. *Chem.—Eur. J.* **2009**, *15*, 8382–8394.
- (11) Walker, D. C.; Chappel, S.; Mahammed, A.; Brunschwig, B. S.; Winkler, J. R.; Gray, H. B.; Zaban, A.; Gross, Z. *J. Porphyrins Phthalocyanines* **2006**, *10*, 1259–1262.
- (12) Agadjanian, H.; Ma, J.; Rentsendorj, A.; Valluripalli, V.; Hwang, J. Y.; Mahammed, A.; Farkas, D. L.; Gray, H. B.; Gross, Z.; Medina-Kauwe, L. K. *Proc. Natl. Acad. Sci.* **2009**, *106*, 6105–10.
- (13) Hwang, J. Y.; Agadjanian, H.; Medina-Kauwe, L. K.; Gross, Z.; Gray, H. B.; Sorasaenee, K.; Farkas, D. L. *Proc. SPIE* **2008**, 6859.
- (14) Luobeznova, I.; Raizman, M.; Goldberg, I.; Gross, Z. *Inorg. Chem.* **2005**, *45*, 386–394.
- (15) Barata, J. F. B. *Química* **2010**, *118*, 23–26.
- (16) Samaroo, D.; Vinodu, M.; Chen, X.; Drain, C. M. *J. Comb. Chem.* **2007**, *9*, 998–1011.
- (17) Hwang, J. Y.; Lubow, J.; Chu, D.; Ma, J.; Agdjanian, H.; Sims, J.; Gray, H. B.; Gross, Z.; Farkas, D. L.; Medina-Kauwe, L. K. *Mol. Pharmaceutics* **2011**, *8*, 2233–2243.
- (18) Flamigni, L.; Gryko, D. T. *Chem. Soc. Rev.* **2009**, *38*, 1635–1646.
- (19) Haber, A.; Mahammed, A.; Fuhrman, B.; Volkova, N.; Coleman, R.; Hayek, T.; Aviram, M.; Gross, Z. *Angew. Chem., Int. Ed.* **2008**, *47*, 7896–900.
- (20) Haber, A.; Aviram, M.; Gross, Z. *Chem. Sci.* **2011**, *2*, 295–302.
- (21) Balazs, Y. S.; Saltsman, I.; Mahammed, A.; Tkachenko, E.; Golubkov, G.; Levine, J.; Gross, Z. *Magn. Reson. Chem.* **2004**, *42*, 624–635.
- (22) Mahammed, A.; Gross, Z. *J. Inorg. Biochem.* **2002**, *88*, 305–309.
- (23) Kowalska, D.; Liu, X.; Tripathy, U.; Mahammed, A.; Gross, Z.; Hirayama, S.; Steer, R. P. *Inorg. Chem.* **2009**, *48*, 2670–2676.
- (24) Liu, X.; Mahammed, A.; Tripathy, U.; Gross, Z.; Steer, R. P. *Chem. Phys. Lett.* **2008**, *459*, 113–118.
- (25) Wagnert, L.; Berg, A.; Stavitski, E.; Berthold, T.; Kothe, G.; Goldberg, I.; Mahammed, A.; Simkhovich, L.; Gross, Z.; Levanon, H. *Appl. Magn. Reson.* **2006**, *30*, 591–604.
- (26) Frisch, M. J.; Trucks, G. W.; Schlegel, H. B.; Scuseria, G. E.; Robb, M. A.; Cheeseman, J. R.; Scalmani, G.; Barone, V.; Mennucci, B.; Petersson, G. A.; et al. *Gaussian 09*; Gaussian, Inc.: Wallingford CT, 2009.
- (27) Kohn, W.; Sham, L. *J. Phys. Rev.* **1965**, *140*, A1133–1138.
- (28) Runge, E.; Gross, E. K. U. *Phys. Rev. Lett.* **1984**, *52*, 997–1000.
- (29) Ghosh, A.; Wondimagegn, T.; Parusel, A. B. *J. Am. Chem. Soc.* **2000**, *122*, 5100–5104.
- (30) Bendix, J.; Dmochowski, I. J.; Gray, H. B.; Mahammed, A.; Simkhovich, L.; Gross, Z. *Angew. Chem., Int. Ed.* **2000**, *39*, 4048–4051.
- (31) George, S. D.; Hocking, R. K.; Gross, Z.; Walker, F. A.; Hodgson, K. O.; Hedman, B.; Solomon, E. I. *Inorg. Chem.* **2009**, *48*, 1678–1688.
- (32) Linke, M.; Lauer, A.; von Haimberger, T.; Zacarias, A.; Heyne, K. *J. Am. Chem. Soc.* **2008**, *130*, 14904–14905.
- (33) Theisen, M.; Linke, M.; Kerbs, M.; Fidder, H.; Madjet, M. E. A.; Zacarias, A.; Heyne, K. *J. Chem. Phys.* **2009**, *131*, 124511.
- (34) Kaindl, R. A.; Wurm, M.; Reimann, K.; Hamm, P.; Weiner, A. M.; Woerner, M. *J. Opt. Soc. Am. B* **2000**, *17*, 2086–2094.
- (35) Lim, M.; Jackson, T. A.; Anfinrud, P. A. *Science* **1995**, *269*, 962–966.
- (36) Zemojtel, T.; Rini, M.; Heyne, K.; Dandekar, T.; Nibbering, E. T. J.; Kozlowski, P. M. *J. Am. Chem. Soc.* **2004**, *126*, 1930–1931.
- (37) Wasbotten, I. H.; Wondimagegn, T.; Ghosh, A. *J. Am. Chem. Soc.* **2002**, *124*, 8104–16.
- (38) Joffre, M.; Hulin, D.; Migus, A.; Antonetti, A.; Laguillaume, C. B. A.; Peyghambarian, N.; Lindberg, M.; Koch, S. W. *Opt. Lett.* **1988**, *13*, 276–278.
- (39) Hamm, P. *Chem. Phys.* **1995**, *200*, 415–429.
- (40) Wynne, K.; Hochstrasser, R. M. *Chem. Phys.* **1995**, *193*, 211–236.
- (41) Nuernberger, P.; Lee, K. F.; Bonvalet, A.; Polack, T.; Vos, M. H.; Alexandrou, A.; Joffre, M. *Opt. Lett.* **2009**, *34*, 3226–32288.
- (42) Roelofs, T. A.; Lee, C. H.; Holzwarth, A. R. *Biophys. J.* **1992**, *61*, 1147–1163.
- (43) Aviv-Harel, I.; Gross, Z. *Coord. Chem. Rev.* **2011**, *255*, 717–736.